

Physics 371 Final Paper:

CMB Polarization Singularities

Nathan C. Keim

June 2, 2006

Abstract

A recent paper by Dragan Huterer¹ and Tanmay Vachaspati [1] discusses a lesser-known method of analyzing the polarization of the CMB: identifying topological defects in the map (points where the polarization vanishes) and examining the statistics of their distribution. The authors look at the statistics for simulated maps with current assumptions about CMB polarization, as well as maps that violate these assumptions. Significantly, they find that, excepting gross anisotropy, these alternative maps hardly change the statistics of singularities. Here, I briefly explain the relevance of CMB polarization measurements to cosmological models, and review prior work on topological defects in the polarization map, before discussing these recent results and their significance.

¹Since the publication of his paper, Dragan Huterer has joined the Chicago KICP as a postdoctoral fellow.

1 Introduction

Small-scale vacuum fluctuations before inflation, and during its early stages, are frozen as they grow larger than the horizon, then return as fluctuations on observable scales [2, 3, 4]. These fluctuations are ultimately responsible for structure formation in the universe. A wide variety of inflationary models can account for the large-scale structure we see today. However, the fluctuations are also manifest as acoustic waves at the time of last scattering, of which the cosmic microwave background (CMB) provides a snapshot. Studying the angular scales of temperature anisotropies of the CMB, first detected in 1992, as well as its linear polarization, allows us to reconstruct the spectrum of primordial fluctuations and the history of inflation. Even more sensitive observations of polarization may yield a spectrum of primordial gravitational waves — which are not responsible for structure, but would give further clues about the early universe.

1.1 CMB Polarization

Some of the CMB radiation is linearly polarized, thanks to the fact that most electrons at the surface of last scattering see a quadrupole temperature anisotropy around them (see Figure 1) [5, 4]. Polarization that is correlated with temperature anisotropies was first reported in 2002 by the DASI experiment; most recently, the WMAP experiment has fully established this correlation over a large area of the sky [6].

Observations of linear polarization are often described in terms of the orthogonal Stokes

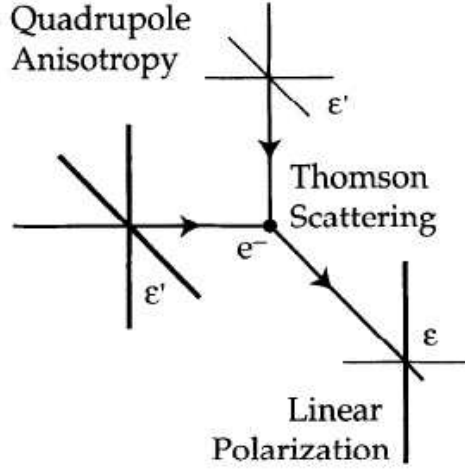


Figure 1: An electron on the surface of last scattering emits linearly polarized radiation according to the quadrupole moment of its thermal environment. Thicker lines represent more intense radiation. Reproduced from Figure 1 of [5].

parameters Q and U , which may be defined as

$$Q = I \cos(2\alpha), \quad U = I \sin(2\alpha) \quad (1)$$

where I is the intensity of the polarized radiation, and α is the polarization angle [7]. The coordinate system for Q , U , and α is established on the sky according to one of several conventions.

The physically relevant polarization that we expect in the CMB can be broken down into two types, based on the underlying classes of perturbations:

E mode polarization has vectors radially or tangentially oriented around CMB hot and cold spots. This comes from ordinary scalar (*i.e.* structure-forming) perturbations in the density. The mechanism for its generation is shown in Figure 2, which considers a component

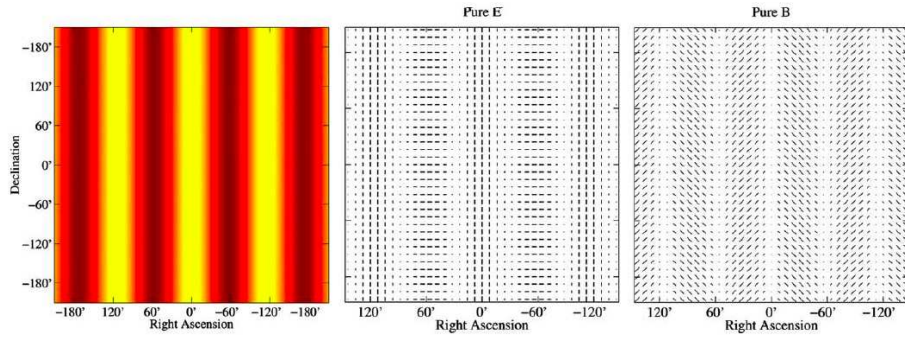


Figure 2: Illustration of E and B polarization modes. **Left panel:** a standing acoustic wave, which is a single Fourier component of the scalar density perturbations. **Center panel:** E -mode polarization comes from the local temperature anisotropy in the acoustic mode, as well as Doppler boosting of radiation from matter as it moves in accordance with the mode. Linear polarization is generated as in Figure 1. **Right panel:** B -mode polarization is at a 45° angle to E -mode polarization, and cannot be generated by scalar perturbations.

of these perturbations.

B mode polarization cannot be produced by scalar perturbations, but can be produced by tensor perturbations (gravitational waves), which distort space but do not alter the density of the plasma. *B* modes are much weaker than *E* modes, and have not yet been detected at angular scales of interest [6].

When many acoustic wave modes due to scalar perturbations — isotropically distributed in direction and with many different phases and amplitudes — are combined on the surface of last scattering, the resulting *E*-mode polarization map is complex and statistically isotropic.

2 Topological Defects in the Polarization Map

Instead of considering the CMB polarization map in relation to the temperature anisotropies, let us consider the angles of linear polarization alone, as a field of headless vectors of uniform magnitude. This approach is informed by what is already known about nematic liquid crystals [7]. Nematic liquid crystals are formed when large numbers of identical rigid rods condense from a liquid phase, where the rods are randomly oriented, to a nematic phase where neighboring rods are nearly parallel [8]. Both the liquid crystal and the polarization map have spatial continuity of the vector orientation angle α , which is their order parameter. The order parameter space is $\mathcal{M} = P_1$, the unit circle with one half mapped onto the other.

Rather than being perfectly globally aligned, these systems typically have topological defects of the types shown in Figures 3 and 4. These defects are also referred to as singularities:

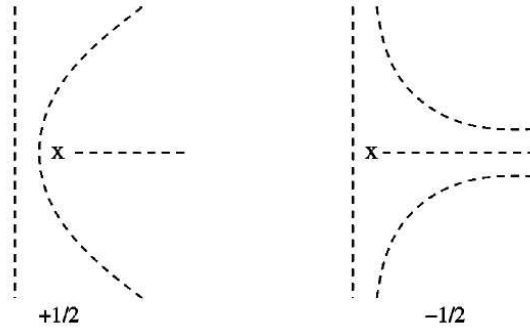


Figure 3: Lone topological defects with charge $k = \pm 1/2$. The vectors around the defect are tangential to the dashed contours. \times is the position of the singularity, where the order parameter is undefined. Reproduced from Figure 1 of [7].

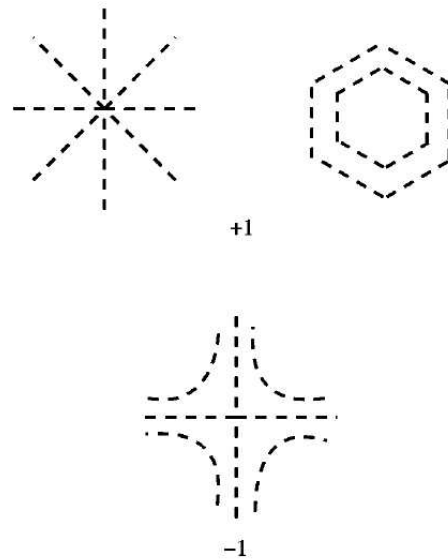


Figure 4: Lone topological defects with charge $k = \pm 1$. These may be formed by combining defects from Figure 3. Reproduced from Figure 2 of [7].

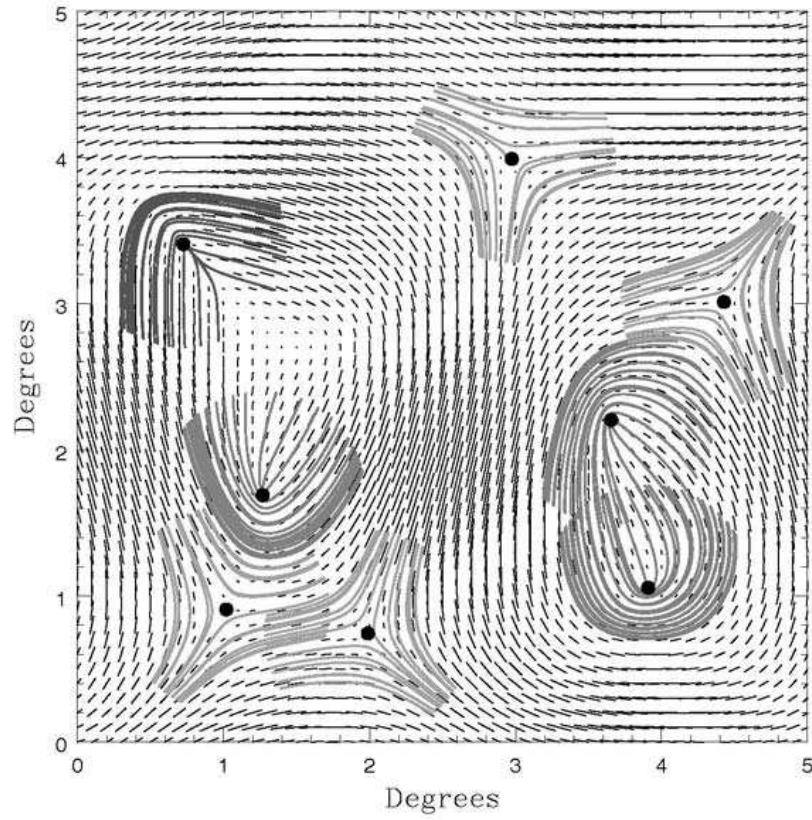


Figure 5: A simulated polarization map of a $5^\circ \times 5^\circ$ region of the CMB. Superimposed on the linear polarization vectors are the singularities in the map, marked with dots, and shown with surrounding polarization directions as in Figures 3 and 4. Reproduced from Figure 4 of [9].

they have a central point where the order parameter is undefined, and immediately around which the derivative of the order parameter diverges. In the case of the polarization map, radiation from the singular point is unpolarized. The singularities in a simulated CMB polarization map are shown in Figure 5.

A lone defect is topologically stable: because the order parameter must be continuous everywhere but at the defect, the defect is “locked in.” Removing it by smoothly reorienting vectors requires changes arbitrarily far from the singularity, and therefore no non-global process that keeps the order parameter continuous in space and time can do so. However, two oppositely charged defects can come together and annihilate.

These and other properties of topological defects are formalized by considering the contour integral

$$\oint d\alpha = \oint_{\Gamma} \frac{d\alpha}{ds} ds = 2k\pi \quad (2)$$

where $k = 0, \pm 1/2, \pm 1, \dots$ is called the winding number or charge [8]. This integral measures the amount of continuous rotation of the vector angle α as the closed contour Γ is traversed²; the value of k is restricted to half-integers because the contour ends with a (headless) vector of the same orientation with which it began. Like Gauss’s law, Equation 2 finds the net charge inside the contour — the sum of the winding numbers of the individual defects that are enclosed. Figures 3 and 4 show examples of individual singularities with charge $\pm 1/2$ and ± 1 .

The paper by Huterer and Vachaspati [1] employs four kinds of analysis, introduced below.

²To evaluate this integral on a sphere, the vectors along Γ must first be moved, by parallel transport, to a common point chosen inside Γ [7].

2.1 Density of singularities

One simple kind of analysis involves counting all singular points on the map, or counting singularities of each k separately. This may be done observationally by looking for a pattern of polarization in the vicinity of a singularity, rather than searching for points where the polarization vanishes [9].

Naselsky and Novikov [10] have predicted this density for a Gaussian polarization field. In such a field, the Q and U Stokes parameters and their first spatial derivatives fluctuate independently, with a Gaussian distribution about zero that has variance σ_0 for Q and U , and σ_1 for the derivatives. Fluctuations in the CMB are widely assumed to be Gaussian, being the sum of many statistically isotropic modes with uncorrelated phases [2], and recent observations have not seriously undermined this assumption [11]. Naselsky and Novikov calculate the density of singularities based on the probability that at a given point, $Q = U = 0$. The density of a single type of singularity can also be calculated by using a criterion for the values of the first spatial derivatives at that point [10, 12]. These authors define a correlation radius $r_c = \sigma_0/\sigma_1$ for the map, and find that the total number density of singularities is $1/4\pi r_c^2$. They note that the density ratios among the different types of singularities depend solely on the Gaussianity of the polarization fields, and that measuring these densities on the sky would test for non-Gaussianity in the CMB. A subsequent paper [9] uses a more refined classification scheme that is compatible with the winding number-based scheme of [1, 7]. This analysis finds that $k = +1/2$ and $k = -1/2$ defects are equally likely, as must hold approximately on a spherical map, which

always has net charge $+2$ [1, 7].

The above analysis assumes perfect Gaussian distributions for every point of the polarization map. Vachaspati and Lue [7] note that the polarization map is constrained by the prevalence of E modes, and that intuitively one might expect this to alter the map's statistics. However, they point out that it is the intensity of polarized radiation, together with the directions of the polarization, that determine the E vs. B composition, and that the directions by themselves, and therefore the distribution of singularities, are not influenced by the composition.

2.2 Scaling of the RMS of enclosed charge

If we take the map to have a correlation length ξ , so that regions separated by more than ξ fluctuate independently of each other, then we may choose a contour Γ with a length $L \gg \xi$, enclosing many such independent regions [7]. The integral in Equation 2 for such a contour is therefore a sum of random, uncorrelated Gaussian fluctuations, and its value k will vary depending on which contour is chosen. If the contour has length L , then the integral samples L/ξ independent fluctuations. The RMS variance of k over many such contours should therefore scale as $\sqrt{L/\xi}$. This result is expressed as the power law

$$k_{\text{RMS}} \equiv \langle k^2 \rangle^{1/2} \propto \left(\frac{L}{\xi} \right)^\beta \quad (3)$$

where the angle brackets denote the average over many contours of length L , and $\beta = 1/2$ is a universal scaling exponent. Vachaspati and Lue [7] point out that the CMB is thought to have negligible spatial correlation above a few degrees. Testing Equation 3 on the CMB polarization

map should therefore test assumptions about spatial correlation and the nature of fluctuations in the CMB. This measurement is independent of the angular correlations in Q and U that are typically used to characterize the polarization map, since the analysis is of polarization direction only, and discards the information in $\sqrt{Q^2 + U^2}$.

Meaningful analysis of polarization may thus be exclusively spatial, without consideration of the spherical harmonics that are crucial to analyzing temperature anisotropy. Purely spatial analysis has the considerable advantage of being more robust with regard to foregrounds: when we mask regions of the sky to eliminate foregrounds, the analysis method is essentially unchanged [1]. This method should also work independently of map resolution, provided that many contours with $L \gg \xi$ are possible.

Furthermore, unless foreground objects introduce their own polarization singularities, they cannot alter the charge distribution of the map, except on the smallest scales. This robustness is thanks to the topological stability of defects, whereby any continuous process cannot change the net charge of a region — a process such as Faraday rotation, or weak gravitational lensing [7].

2.3 Nearest-neighbor distance of singularities

Another spatially-based analysis, though less robust to distortions of the map, is the measurement of the distance from a singularity to its nearest neighbor of equal charge, and also to its nearest neighbor of equal and opposite charge [1].

2.4 Angular power spectrum of singularities

Huterer and Vachaspati [1] also consider the related analysis of the two-point correlation function for defects: the excess probability, above that predicted by a completely random distribution, that singularities will be found at both positions $\vec{\theta}_1$ and $\vec{\theta}_2$ on the sky. Assuming statistical isotropy, the two-point correlation function is $w(\theta)$ for $\theta = |\vec{\theta}_1 - \vec{\theta}_2|$, and enters into the two-point probability as

$$dP(\vec{\theta}_1, \vec{\theta}_2) = dP(\vec{\theta}_1)dP(\vec{\theta}_2)(1 + w(\theta)) \quad (4)$$

3 Computational Results of Huterer and Vachaspati

Huterer and Vachaspati [1] performed the analyses described in Section 2 on several simulated CMB polarization maps. They started with maps produced from a fiducial Λ CDM cosmology, including a flat universe, matter energy density $\Omega_M = 0.3$, cosmological constant-style dark energy ($w = -1$), and scale-invariant perturbations ($n_s = 1$). Tensor modes in the CMB, due to primordial gravitational waves, were taken to be negligible, and omitted.

3.1 Results for a fiducial model

The total number of singularities N_{sin} was found to depend strongly on the resolution of the map, scaling with maximum resolution l_{max} approximately as l_{max}^2 , as we would expect from the scale-free character of point defects, and consistent with the prediction of Naselsky and Novikov [10], stated earlier, that density scales with the correlation radius as r_c^{-2} . At lower

resolutions, oppositely charged defects are apparently combined by coarse-graining, preserving winding number but diminishing N_{sin} . The authors estimate that, since the actual map is thought to have power out to $l \sim 2000$, a map with perfect resolution would have over a million singularities. However, they state that none of the analyses they use requires resolution on such small angular scales.

The authors then tested the scaling of law of Equation 3, for RMS charge inside a contour as a function of the contour's length. Their algorithm used randomly chosen rings on the sky. Interestingly, they found that the scaling exponent β , expected to have a universal value of $1/2$ [7], instead varies slightly with map resolution, as shown in Figure 6 — although this conclusion appears to rely heavily on data gathered for the smallest L .

Huterer and Vachaspati [1] next measured the distribution of nearest-neighbor distances among the singularities. Assuming a resolution $l_{\text{max}} = 100$, they found that the distributions for distance to the nearest neighbor of equal charge, and to the nearest neighbor of opposite charge, were unimodal, with means of 3.24° and 2.69° respectively.

The authors finally tested the angular power spectrum of singularities, with the finding that the correlation function $w(\theta)$ is zero for $\theta \gtrsim 1^\circ$. At small angles, $w(\theta)$ reflects the findings for nearest-neighbor distance.

3.2 Results for alternate models

Huterer and Vachaspati [1] also performed the same analyses on maps generated from alternate cosmological models. The following variations were employed:

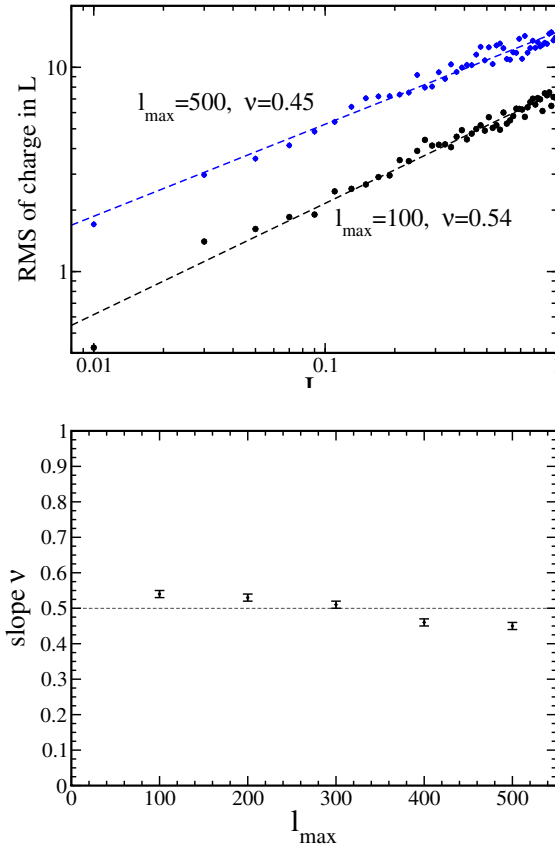


Figure 6: Test of the scaling of RMS enclosed charge. **Upper panel:** Scaling of the RMS charge enclosed in a contour with the contour's length L , for two different map resolutions. **Lower panel:** The scaling exponent β (here labeled as v) as a function of the maximum resolution of a simulated CMB map. The exponent is close to the universal value of $1/2$, but varies slightly with resolution. Reproduced from Figure 4 of [1].

1. Introducing tensor perturbations 10 times stronger than the scalar perturbations. They are currently thought to be no stronger than 0.28 of scalar perturbations [6].
2. Changing the spectral index n_s of scalar perturbations from 1 to 0 or 2. This could be the result of a mechanism for generating fluctuations that changes significantly as inflation proceeds [2].
3. Making temperature anisotropy maps with strongly non-Gaussian fluctuations: the coefficients of spherical harmonics were chosen from an exponential distribution with the same mean and variance as before.
4. Grossly breaking statistical isotropy, by using only spherical harmonics with $m = 0$ to make the temperature map.

All of these scenarios are mostly or entirely ruled out by observations, though more moderate versions of them are possible (see, *e.g.*, [11]). But despite their extreme nature, all but the fourth one hardly change the statistics from their fiducial values.

4 Discussion

The result, stated above, that singularities of equal charge appear to repel, and those of opposite charge appear to attract, appears to be new and deserves attention. In the analogous system of a nematic liquid crystal, defects may migrate to lower the system's free energy, with just such a local interaction [8]. Huterer and Vachaspati do not speculate on the possible physical

significance of this behavior in the CMB, though we might begin by considering the position of a singularity to be a function of its local polarization field, and not the other way around. This might permit the notion of neighboring singularities “interacting” without the system ever evolving.

Most significantly, the authors found that the statistics of polarization singularities, unlike most other characterizations of the CMB, are insensitive to major changes in the underlying cosmology. The authors find this especially surprising in the case of a large departure from Gaussianity, since Gaussian fluctuations were a key assumption in much of the theory described in Section 2. Indeed, multiple papers [10, 12, 9, 7] proposed the analysis of polarization singularities as a robust way to uncover non-Gaussianity in the CMB.

Confronted with the apparent irrelevance of cosmological parameters to their analysis, Huterer and Vachaspati suggest that the statistics of singularities might yet serve as probes of foreground sources or other systematic errors. They also note that other deviations from their fiducial assumptions, including further forms of non-Gaussianity, might turn out to affect the statistics significantly. No observation has yet produced a sufficiently sensitive polarization map of the CMB covering a significant portion of the sky — data that would likely yield important results from analysis techniques already in use. When such data becomes available, the actual value of these alternate methods might be fully known.

References

- [1] D. Huterer and T. Vachaspati. Distribution of singularities in the cosmic microwave background polarization. *Phys. Rev. D*, 72:043004, 2005.
- [2] S. Carroll. Physics 371 lectures, Spring 2006.
- [3] E.W. Kolb and M.S. Turner. *The Early Universe*. Westview, 1990.
- [4] J.E. Carlstrom, J. Kovac, E.M. Leitch, and C. Pryke. Status of CMB polarization measurements from DASI and other experiments. *New Astr. Rev.*, 47:953, 2003.
- [5] W. Hu and M. White. A CMB polarization primer. *New Astronomy*, 2:323, 1997.
- [6] L. Page, G. Hinshaw, E. Komatsu, M. R. Nolta, D. N. Spergel, C. L. Bennett, C. Barnes, R. Bean, O. Doré, M. Halpern, R. S. Hill, N. Jarosik, A. Kogut, M. Limon, S. S. Meyer, N. Odegard, H. V. Peiris, G. S. Tucker, L. Verde, J. L. Weiland, E. Wollack, and E. L. Wright. Three Year Wilkinson Microwave Anisotropy Probe (WMAP) Observations: Polarization Analysis. *ArXiv Astrophysics e-prints*, March 2006.
- [7] T. Vachaspati and A. Lue. Topological properties of the cosmic microwave background polarization map. *Phys. Rev. D*, 67:121302, 2003.
- [8] P.M. Chaikin and T.C. Lubensky. *Principles of Condensed Matter Physics*. Cambridge U. P., 1995.

- [9] A. Dolgov, A. Doroshkevich, D.I. Novikov, and I.D. Novikov. Geometry and statistics of cosmic microwave polarization. *Int. J. Mod. Phys. D*, 8:189, 1999.
- [10] P.D. Naselsky and D.I. Novikov. General statistical properties of the cosmic microwave background polarization field. *ApJ*, 507:31, 1998.
- [11] D. N. Spergel, R. Bean, O. Doré, M. R. Nolta, C. L. Bennett, G. Hinshaw, N. Jarosik, E. Komatsu, L. Page, H. V. Peiris, L. Verde, C. Barnes, M. Halpern, R. S. Hill, A. Kogut, M. Limon, S. S. Meyer, N. Odegard, G. S. Tucker, J. L. Weiland, E. Wollack, and E. L. Wright. Wilkinson Microwave Anisotropy Probe (WMAP) Three Year Results: Implications for Cosmology. *ArXiv Astrophysics e-prints*, March 2006.
- [12] A. Dolgov, A. Doroshkevich, D.I. Novikov, and I.D. Novikov. Classification of singular points in the polarization field of the cosmic microwave background and eigenvectors of the stokes matrix. *JETP Lett.*, 69:427, 1999.